

Particle control and SOL plasma flow in the W-shaped divertor of JT-60U

N Asakura, H. Takenaga, K Shimizu, S. Sakurai, H. Tamai, A. Sakasai

Naka Fusion Research Establishment

Japan Atomic Energy Research Institute

Naka-machi, Naka-gun, Ibaraki-ken, Japan

Abstract. The divertor pumping is a fundamental tool for particle control in the fusion reactor. Effect of the divertor pumping on the SOL plasma and impurity ions has been studied in many divertor tokamaks. Recent experiment studies of particle exhaust and the SOL flow study in the JT-60U are summarized. Pumping flux at the inner and outer pumping slots of the W-shaped divertor were investigated under the attached and detached divertor conditions. Reciprocating Mach probes have measured the plasma flow in the Low-field-side SOL (midplane and divertor x-point), and new Mach probe was installed at the high-field-side SOL. The SOL flow pattern and preliminary results of SOL simulation introducing the ion drifts were summarized.

1. Introduction

The divertor pump is a fundamental tool for particle control in the fusion reactor. Compact design of the pump divertor is essential, and, at the same time, the following performance should be satisfied: (1) sustainment of the detached divertor to reduce target heat load, (2) helium ash exhaust from the improved confinement plasma, and (3) efficient impurity shielding from the main plasma. The divertor performance is influenced not only by the pumping speed but also by the plasma profile and flow pattern in the SOL and divertor. Understanding of plasma and neutral transport in the different geometries of the pump divertor is of great importance for optimizing the design of divertor and pump system.

Effective pumping speed and its influences on the divertor performance have been studied in the compact W-shaped divertor of JT-60U[1, 2]. Effects of the divertor geometry on the heat and particle transport in the SOL were investigated using intensive divertor diagnostics such as Langmuir probes, infrared TV camera, divertor ion gauges, bolometer arrays and spectroscopy system[3, 4, 5]. Multi-point measurement of the plasma flow has been developed in order to find out fundamental problems of the particle transport, such as Mach number and in-out asymmetry in particle flux in torus. In the first part of this paper, effective pumping speed in the W-shaped divertor is investigated, and effects of the pumping on the particle control are summarized. In the second part, results of the plasma flow measurements using three Mach probes and UEDGE simulations introducing the ion drifts are shown.

2. Private pumping in the W-shaped divertor

The compact W-shaped divertor started from 1997 (May) as shown in Fig. 1. A dome separates the private flux region, and neutrals are exhausted from the inner and outer slots of the private flux region, i.e. Both-side-Pumping (B-s-P). The pumping slots of 3 cm (inner) and 2 cm (outer) widths are arranged between the divertor plates and the wings of the dome. Three pumping ports (ϕ 0.6 m \times 4.8 m) are connected to the duct under the baffle. Cryopumps with pumping speed of 1000 m³/s each are used for divertor pumping. Gas fueling valves are mainly used at the top of the vacuum vessel. Separations of the inner/outer strike-point from each pumping slot, δ_{gap-In} and $\delta_{gap-Out}$, are important parameters to determine the effective pumping speed.

At the start (in 1997 and 1998), the outer slot was closed in order to evaluate the pumping speeds at the inner divertor. Net pumping speed for the Inner-side-Pumping (I-s-P) is 13 m³/s in molecular flow. The reduction in pumping speed is mainly attributed to conductance of pumping ports and narrow gaps from the dome to the outer sub-divertor (common exhaust slot). The recycling flux was greatly enhanced in the inner divertor, compared to that at the outer divertor for the ion ∇B drift towards the divertor. The pumping in the high recycling divertor was demonstrated.

The outer slot has been opened since 1999. At the same time, dome tiles were replaced from graphite to CFC for the higher thermal strength, which allowed closure gap operation. The measured net pumping speed at the pumping slot in the divertor is increased to be 17 m³/s in molecular flow.

2.1. neutral leak in Both-side-Pumping

Leak of neutrals was anticipated for B-s-P due to in-out asymmetries of recycling and separations, δ_{gap-In} and $\delta_{gap-Out}$. Effect on the pumping speed was investigated in Ref. [6], and the pumping fluxes for B-s-P and I-s-P, and leak neutral flux for B-s-P were evaluated using the UEDGE-DEGAS2 code.

Pumping flux, Φ_{pump} , was deduced from the difference of gas puff rates, $\Phi_{gas}^{pump-ON}$ and $\Phi_{gas}^{pump-OFF}$, for the cases of opening and closing the cryopump shutters, respectively. The particle balance is represented as the equations; $\Phi_{gas}^{pump-ON} + \Phi_{NB} = \Phi_{absorb} + \Phi_{pump}$ for the pumping case, and $\Phi_{gas}^{pump-OFF} + \Phi_{NB} = \Phi_{absorb}$ for the pumping off case. Here, Φ_{NB} and Φ_{absorb} are injected particle flux by neutral beam injection and absorbed flux to the divertor and first wall, respectively. Pumping flux is deduced from $\Phi_{gas}^{pump-ON} - \Phi_{gas}^{pump-OFF}$ under the steady discharge conditions at the same plasma density and similar recycling flux. The same Φ_{absorb} is assumed. Parameters of ELMY H-mode plasma are $I_p = 1.0/1.5$ MA, the toroidal magnetic field $B_t = 3.5/3.8$ T with the ion ∇B drift direction towards the divertor target, $q_{95} = 4$, and NBI power $P_{NBI} = 11$ MW.

Pumping flux is normalized by volume integral of D_α brightness, $I_{D_\alpha}^{Total}$, which approximately corresponds to total ionization flux, $\Phi_{recycle}$, assuming the photon emission rate coefficient such as 15 [7]. Pumping flux ratios, $\Phi_{pump}/I_{D_\alpha}^{total}$, for the cases of B-s-P and I-s-P are compared in Fig. 2 as a function of recycling flux ratio of the inner and outer divertors, $I_{D_\alpha}^{In}/I_{D_\alpha}^{Out}$. Detached and attached divertor cases are chosen for the different combination of I_p and B_T . Separation of δ_{gap-In} and $\delta_{gap-Out}$ are fixed

at 3–3.5 cm. Under the attached divertor condition, pumping flux ratios for B-s-P are a factor of $1/6$ – $1/4$ smaller than those for I-s-P. Since the in-out asymmetry in recycling profile is enhanced as shown in Fig. 2(b), the pumping flux ratio is reduced due to neutral leak from the inner divertor to the outer divertor. During the x-point MARFE, recycling flux at the outer divertor is greatly increased and symmetric profile is observed as shown in Fig. 2(c). Pumping ratio for B-s-P is increased under a partially detached divertor condition, which suggests an increase in the pumping flux at the outer divertor.

Pumping flux ratio, $\Phi_{pump}/\Phi_{recycle}$, can be improved for the divertor closure operation with decreasing δ_{gap-In} and $\delta_{gap-Out}$. Figure 3 shows pumping flux ratios as a function of δ_{gap-In} (for I-s-P) or $\delta_{gap-Out}$ (δ_{gap-In} is comparable value for B-s-P, except for $\delta_{gap-Out} = 6$ cm and $\delta_{gap-in} = 3$ cm). Pumping flux ratio for the small-gap of 0.5 cm is increased a factor of 3–4 larger than those for wider $\delta_{gap-Out}$.

Simulation of leak and pumping flux ratios are performed under the attached divertor condition using UEDGE-DEGAS2 code[8, 9]. Edge plasma parameters were determined to reproduce the measured density and temperature profiles at the edge and SOL. The background plasma model was fixed without iterative calculations between UEDGE and DEGAS2. Pumping and leak fluxes were calculated with varying pumping ratio at the common exhaust slot, f_{pump} , from 0 to 0.5. Net pumping and leak fluxes at the inner, outer and common exhaust slots are shown in Fig. 4 for two cases; $\delta_{gap-In} = \delta_{gap-Out} = 3$ cm, and closure operation ($\delta_{gap-In} = 1$ cm and $\delta_{gap-Out} = 0.5$ cm), where f_{pump} is 0.1. For the closure gap operation, leak neutral flux ratio at the outer slot can

be minimized from 1.4% to 1.1% of $\Phi_{recycle}$. Net pumping ratio at the common exhaust slot is increased from 0.95 to 1.56% of $\Phi_{recycle}$. However, net pumping at the outer slot was not seen with increasing f_{pump} up to 0.5. Since the conductance at the common exhaust slot limits the net pumping speed, wider common pumping slot will improve the pumping performance. Or separated pumping system will be preferable to obtain maximum pumping under the condition of large in-out asymmetry in recycling flux.

2.2. performance for closure operation of B-s-P

Sustainment of the detached plasma without causing the x-point MARFE, “detached divertor”, is crucial for the divertor operation. For the closure operation of B-s-P, the maximum plasma density for the detached divertor was extended to be higher than those for the wider gap operation of B-s-P and I-s-P[3, 5] Deuterium pressures at inner and outer divertor are measured using fast-response ion gauges[5], in the attached and detached divertor for B-s-P and I-s-P, where the plasma is L-mode, $I_p = 1.2$ MA, $B_t = 3.5$ T, $P_{NBI} = 4.3$ MW. For the detached divertor, similar to in-out asymmetry in the D_α brightness, neutral pressure at the inner divertor, p_0^{In} , is maintained at high level, and neutral pressure at the outer divertor, p_0^{Out} , is increased. At the MRARFE onset, p_0^{In} is decreased a little while P_0^{Out} is increase, and in-out asymmetry in p_0 is reversed. Values of p_0^{In} and p_0^{Out} are shown for the different δ_{gap} in Fig. 5. Divertor pumping for the closure operations with the two cases, (1) $\delta_{gap-In} = 0.3$ cm and $\delta_{gap-Out} = 1$ cm and (2) $\delta_{gap-In} = \delta_{gap-Out} = 2$ cm, shows that the partially detached divertor without x-point

MARFE is sustained at higher divertor pressure, and that density range is extended to be higher than cases for larger δ_{gap} . This results suggests that pumping-out both at inner and outer divertors is achieved in the detached divertor.

Helium exhaust efficiency is improved in the closure operation of B-s-P ($\delta_{gap-In} = 1.4$ cm and $\delta_{gap-Out} = 0.8$ cm) [10]. Helium beam was injected into the ELMy H-mode plasma, where $I_p = 1.4$ MA, $B_t = 3.5$ T, $P_{NBI} = 16$ MW and helium pump (cryo-pumping with Ar-frost) is used. Helium beam energy of 60 keV and power of 1.4 MW corresponds to 1.5×10^{20} s⁻¹, equivalent to 85 MW α heating. Helium ion density in the core plasma is saturated at 7×10^{17} m⁻³ for $\bar{n}_e = 3.8 \times 10^{19}$ m⁻³. Helium confinement time ratio, τ_{He}^*/τ_E , is shown in Fig. 6 as a function of \bar{n}_e . At the high density of $\bar{n}_e = 3.4 \times 10^{19}$ m⁻³ τ_{He}^*/τ_E of 4.7 is larger than that 3.9 for I-s-P with $\delta_{gap-In} = 3.5$ cm. With increasing \bar{n}_e , τ_{He}^*/τ_E is improved to 2.8 at $\bar{n}_e = 3.8 \times 10^{19}$ m⁻³ with the closure operation, where $\tau_{He}^* = 0.36$ s and $\tau_E = 0.13$ (ripple loss power of 20% is included in the absorbed power for τ_E calculation). At the density, in-out asymmetry in the recycling profile is observed in the divertor, suggesting that leak at the outer divertor decreases the pumping speed.

3. SOL plasma flow study

The SOL plasma flow is generally considered to be driven along the magnetic field lines from the main plasma edge to the divertor target, which is a strong plasma sink[11]. Control of the plasma flow in SOL and divertor, using a pumping system,

is considered important because of its implications for the exhaust of helium ash and impurity retention in the divertor. The SOL flow pattern is one of the most important factors to determine divertor plasma conditions such as in-out asymmetries in particle and heat fluxes and “flow reversal”, which are not explained by the conventional sheath model. Understanding of the drive mechanism will contribute to optimize the pump divertor design to control plasma and neutrals.

The SOL plasma flow are measured using three reciprocating Mach probes installed at the outer midplane, near the x-point and above the inner baffle plate as shown in Fig.7. In particular, the reciprocating Mach probe above the inner baffle is recently installed, and the SOL plasma profile at the high-field-side was, for the first time, measured in the divertor tokamak. Profiles of ion saturation currents at the up-stream side (midplane side) and down-stream side (divertor side), j_s^{up} and j_s^{down} , electron temperatures, T_e^{up} and T_e^{down} , and floating potential, V_f , are measured with spatial resolution of 1–2 mm[4]. The direction of the plasma flow along the field lines is deduced from the ratio of j_s^{down} to j_s^{up} , i.e. j_s^{down}/j_s^{up} . A value lower than unity indicates a flow directed normally from up-stream to down-stream location along the field lines. Mach number of the plasma flow is evaluated using Hutchinsons formula, $M = 0.35 \ln(j_s^{down}/j_s^{up})$ [12].

Parameters of the L-mode plasma are $I_p = 1.6$ MA, $B_T = 3.3$ T, $q_{95} = 3.5$, $\delta = 0.33$, $P_{NB} = 4.3$ MW, where plasma density changes on shot-by-shot basis for the normal and reversed ion ∇B drift directions. The I_p and B_t are both clockwise in the discharge with the ion ∇B drift towards the divertor, and are both counter-clockwise for the discharge

with the ion ∇B drift away from the divertor.

3.1. SOL flow pattern

The ion ∇B drift direction and plasma density both affect the plasma flow at the main plasma edge. Profiles of Mach number at the midplane, near the x-point, and above the inner baffle are shown in Fig. 8(a) and (b) for the ion ∇B drift directions towards and away from the divertor, respectively. Plasma density $\bar{n}_e = (1.6 - 1.7) \times 10^{19} \text{ m}^{-3}$. The profiles measured with the x-point and inner Mach probes are mapped to the same field lines at the outer midplane radius. Field lines in the SOL width of less than 4 cm are connected to the inner and outer divertors. Positive and negative Mach numbers show the direction towards the outer and inner divertor, respectively.

For the ion ∇B drift towards the divertor (B_T normal), $M = -0.4$ for the outer midplane shows “flow reversal”. At the outer flux surfaces of the midplane SOL, “flow reversal” is decreased gradually to small value, and the SOL flow towards the outer baffle is seen at $\Delta r \geq 6$ cm. On the other hand, the plasma flows from the x-point to the outer divertor with $M = 0.5$. Measurement of the SOL flow at the two locations confirms that flow reversal occurs only at the main plasma edge. This suggests that stagnate between the x-point and the outer midplane. At the high-field-side, the SOL flow towards the inner divertor $M = 0.4$ is observed in the most region. Assuming that there is no local region with low or high plasma pressure, parallel SOL flow may be driven from the outer midplane to the high-field-side. It should be noted that small

“flow reversal” with $M = 0.2$ is observed at or just outside the separatrix (a few mm at midplane radius, and 1 cm in the probe scan distance), where the region is narrower than that observed at the outer midplane (5 cm).

For the ion ∇B drift away from the divertor (B_T reversal), at the outer midplane and near x-point, $M = 0.2$ and 0.3 are observed near the separatrix, respectively. At the high-field-side SOL, $M = -0.2$ is seen. These results show that the SOL plasma is produced from the plasma top to the inner or outer divertor and “flow reversal” is not seen. It should be noted that flow velocity is increased at the outer flux surfaces of both high- and low-field-sides, and M is increased to sub-sonic level larger than those observed for the normal B_T case.

SOL flow velocity changed with increasing \bar{n}_e . Fig. 9(a) show that “flow reversal” at the outer midplane and high-field-side for the ion ∇B drift towards the divertor is decreased gradually with \bar{n}_e . However, SOL flow towards the divertor near the x-point, as shown in Fig. 9(a) and (b), and outer flux surfaced at the high-field-side, as shown in Fig. 9(b), is increased with \bar{n}_e . The SOL flow is evaluated by $M \times j_s$ at the midplane radius of 1 cm, which is shown in Fig. 9(c). The value of $M \times j_s$ near the x-point and at the high-field-side SOL is increased with \bar{n}_e . Increment of $M \times j_s$ at the high-field-side SOL, is larger than that near the x-point (Low-field-side SOL), and the result shows that in-out asymmetry in the SOL flow from the upstream of the divertor will affects an asymmetry in the recycling flux.

3.2. SOL flow mechanism

Our observations are the followings; (1) flow reversal at the outer midplane, where the neutral density is two or three orders of magnitude lower than that in the divertor chamber. (2) the parallel SOL flow just below the x-point always directing towards the target plate. (3) the SOL flow at the outer midplane driven against the ion ∇B drift direction. (4) the SOL flow at the high-field side is driven against the ion ∇B drift direction just near the separatrix, while the SOL flow at the outer flux surfaces is produced always towards the divertor. Those results show that the transport relating to the ion drift motion, rather than the increase in local ionization, plays a role in driving the parallel SOL plasma flow in the main plasma edge.

Another candidate mechanism, i.e. cross-field diffusion of the edge toroidal momentum, was pointed out as a mechanism to drive the parallel SOL flow[13]. Profiles of the ion temperature, T_i , and the toroidal rotation velocity, V_t , were measured with charge-exchange recombination spectroscopy (CXRS). The direction of V_t just inside the separatrix above the outer midplane was opposite to I_p , and V_t was small (i.e. 10–20 km/s corresponding to a Mach number of 0.5-0.1). In the SOL, the direction of the plasma flow at the outer midplane is in the direction of I_p . This result shows that the SOL flow is not influenced by the toroidal rotation inside the separatrix.

A mechanism to produce the flow reversal at the main plasma edge has been proposed based on the in-out asymmetry in the ion drift motion in a torus[14]; $\mathbf{V}_\perp = (\mathbf{E}_r - \nabla p_i / en_i) \times \mathbf{B} / B^2$. From the particle and momentum equations, an in-out

asymmetry in V_{\perp} drives the parallel ion flux (“Pfirsch-Schlüter flow”)[15]. The direction of the ion “Pfirsch-Schlüter flow” is away from the divertor for the ion ∇B drift towards the divertor and vice versa. A quantitative evaluation of the model, using measured E_r , T_i and λ_{T_i} , shows that ion Pfirsch-Schlüter flow in a toroidal magnetic confinement system is consistent with Mach number deduced from measured j_s^{down}/j_s^{up} [16]. However, a change of the flow direction and the large flow velocity at the outer flux surface are not understood so far.

3.3. Drift simulation using UEDGE-code

Quantitative evaluation of the drift motions is required including the real plasma shape and divertor geometry. Recently, ion drift motions have been introduced into two dimensional simulation code of the SOL and divertor plasma. Preliminary results of the calculated Mach number including the drift effects are compared with the measured profiles of the Mach number. Calculation mesh covered the SOL region of the outer 6 cm at the midplane radius.

Figure 10 shows Mach numbers along the poloidal distance from the inner divertor to the outer divertor at 1 cm outside the separatrix. Introducing the drift motions ($\mathbf{E}_r \times \mathbf{B}$, $\nabla \mathbf{B} \times \mathbf{B}$ and diamagnetic drifts), it is found that parallel plasma flow towards the inner divertor appears around the main plasma, and that flow velocity towards the divertor is increased below the x-point.

Radial profiles at the three Mach probe locations are shown in Fig. 11. At the outer

midplane, “flow reversal” ($M = 0.3-0.4$) is comparable to the measurement. SOL flow velocity at the outside flux-surfaces (larger than 2.5 cm) is driven towards the outer divertor, which is narrower than the measured profile (larger than 6 cm). SOL flow velocities above the inner baffle and near the x-point are increased towards the divertor introducing the drift motions. However, Mach numbers ($M \sim 0.2$) are smaller than measurements (0.5). Flow velocity direction towards the divertor changes and the Mach numbers are also increased due to other factors such as impurity level and diffusion coefficient. The modeling works are under progress.

4. Summary

Maximum pumping ratio and improved performance of the divertor were observed in the detached divertor using the Both-side private pumping, provided that closure gap operation was available. Multi-point measurements of the SOL flow and introduction of the drift motions in SOL plasma simulation show that the parallel SOL flow is produced from low-field side to high-field side for normal B_T direction. SOL flow affects in-out asymmetries in plasma and recycling fluxes in the divertor. Quantitative understanding of the SOL flow and neutral/molecule transport in sub-divertor will contribute to a compact divertor design.

Acknowledgements

Works of UEDGE-DEGAS2 simulation were supported by Drs G. D. Porter,

T. D. Rognlien, and M. E. Rensink in LLNL. The authors thank for comments and discussion with JT-60U boundary physics group, and JT-60SC design group.

References

- [1] Hosogane N *et al* 1999 *J. Nucl. Mater.* **266-269** 296
- [2] Hosogane N *et al* 1999 *Proc. 17th Int. Conf. on Fusion Energy* **Vol. 3** (IAEA, Vienna) 903
- [3] Asakura N *et al* 1999 *J. Nucl. Mater.* **266-269** 182
- [4] Asakura N *et al* 1999 *Nucl. Fusion* **39** 1983
- [5] Tamai H *et al* 1999 *Proc. 26th EPS Conf. on Contr. Fusion and Plasma Physics (EPS, Mulhouse)*
23J 409
- [6] Takenaga H *et al* 2001 appears in *Nucl. Fusion*
- [7] Asakura N *et al* 1995 *Nucl. Fusion* **35** 381
- [8] Rognlien T D *et al* 1994 *Plasma Phys.* **34** 362
- [9] Smith G R *et al* 1994 *J. Nucl. Mater.* **220-222** 1024
- [10] Sakasai A *et al* 2001 *Proc. 18th Int. Conf. on Fusion Energy* **Vol. 3** (IAEA, Vienna) 903
- [11] Stangeby P C and McCracken G M 1990 *Nucl. Fusion* **30** 1225
- [12] Hutchinson I H 1988 *Phys. Rev.* **A37** 4358
- [13] Chankin A V 1997 *J. Nucl. Mater.* **241-243** 199
- [14] Chankin A V and Stangeby P C 1994 *Plasma Phys. Control. Fusion* **36** 1485
- [15] Hugill J 1992 *J. Nucl. Mater.* **196-198** 918
- [16] Asakura N *et al* 2000 *Phys. Rev. Lett.* **84** 3093

Figure captions

Figure 1. JT-60U W-shaped divertor with inner and outer private pumping

Figure 2. (a) Pumping flux ratio, $\Phi_{pump}/I_{D_\alpha}^{total}$, for B-s-P and I-s-P as a function of in-out asymmetry factor, $I_{D_\alpha}^{In}/I_{D_\alpha}^{Out}$. δ_{gap-In} and $\delta_{gap-Out}$ are fixed at 3 cm. Comparisons of D_α brightness profiles in the divertor, (b) for B-s-P and I-s-P (attached divertor), (c) for attached and detached divertor cases.

Figure 3. Pumping flux ratio, $\Phi_{pump}/\Phi_{recycle}$, as a function of δ_{gap-In} (I-s-P) or $\delta_{gap-Out}$ (B-s-P), in attached and detached divertor.

Figure 4. Pumping and leak fluxes, and the ratios normalized by total recycling, $\Phi_{pump}/\Phi_{recycle}$, in the Both-side-Pumping divertor. (a) for $\delta_{gap-Out} = \delta_{gap-In} = 3$ cm, (b) for $\delta_{gap-Out} = 0.5$ cm, $\delta_{gap-In} = 1$ cm.

Figure 5. p_0^{In} and p_0^{Out} for different $\delta_{gap-Out}$ and δ_{gap-In} for B-s-P. I-s-P cases is also shown. X-point MARFE occurs when p_0^{In} is decreased, and p_0^{Out} increased.

Figure 6. The ratio of τ_{He}^*/τ_E as a function of \bar{n}_e . Three cases for wider gap ($\delta_{gap-Out} = \delta_{gap-In} = 4$ cm), closure gap ($\delta_{gap-Out} = 0.5$ cm, $\delta_{gap-In} = 1$ cm) for B-s-P, and $\delta_{gap-In} = 1$ cm for I-s-P are shown.

Figure 7. Plasma cross-section and locations of reciprocating Mach probes at outer midplane, near x-point. New Mach probe is installed above the inner baffle.

Figure 8. Profiles of Mach number measured at the three reciprocating Mach probes (at outer midplane, near x-point and above inner baffle). Here, ion ∇B drift direction, (a) towards the divertor, and (b) away from the divertor.

Figure 9. Mach numbers, (a) near separatrix, and (b) at the outer flux surfaces as a function of \bar{n}_e for the ion ∇B drift towards the divertor. (c) SOL flow flux $M \times j_s$ is shown.

Figure 10. Distributions of the Mach numbers as a function of poloidal distance from the inner divertor. Drift magnitudes of 20% and 80% are introduced.

Figure 11. Profiles of Mach number (a) above the inner baffle, (b) at the outer midplane, (c) near the x-point (low-field-side SOL).

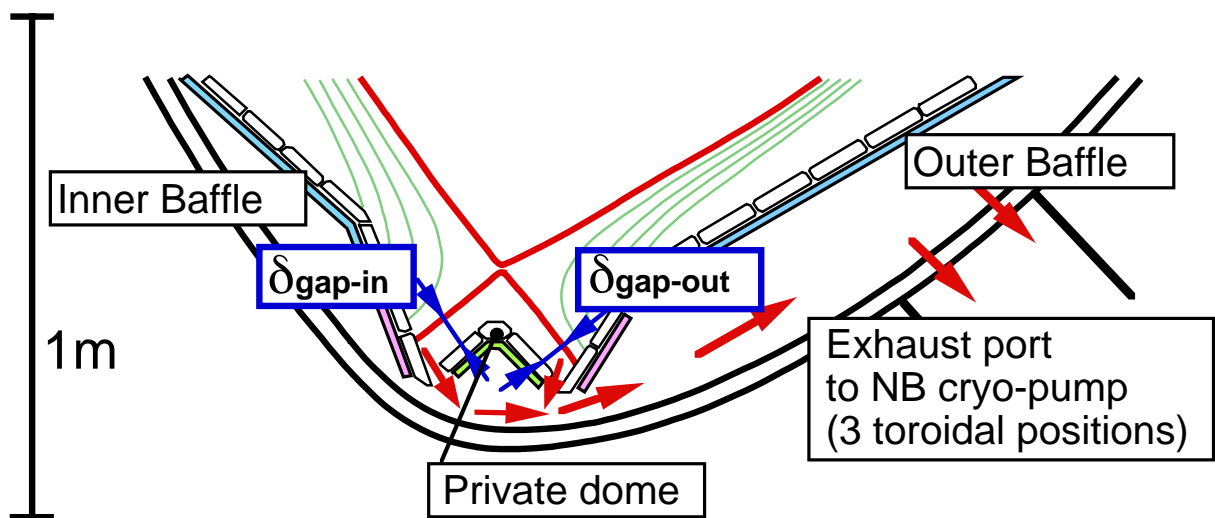


Fig. 1 asakura

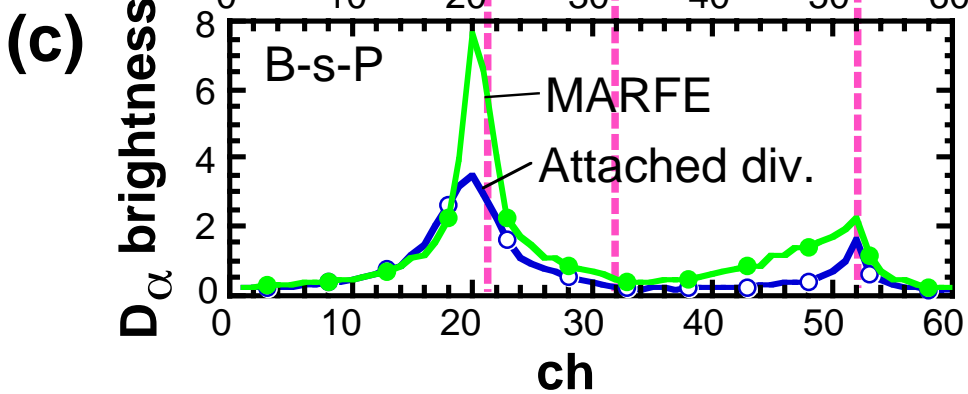
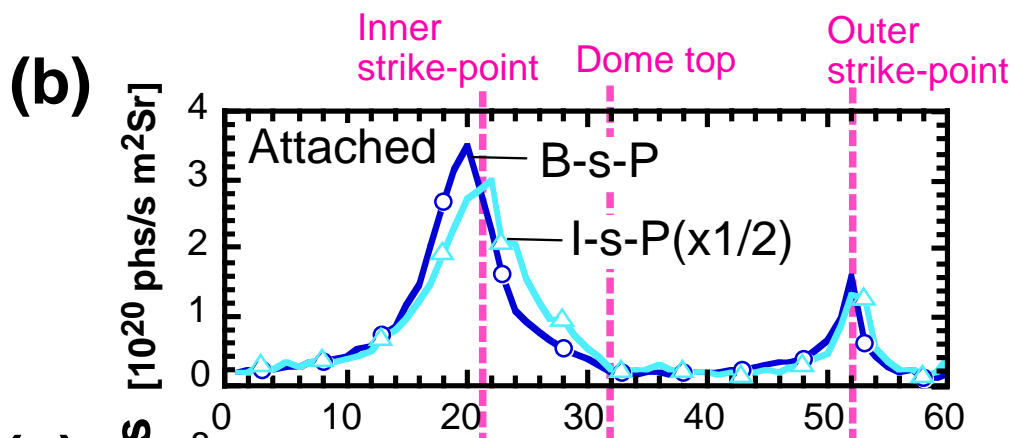
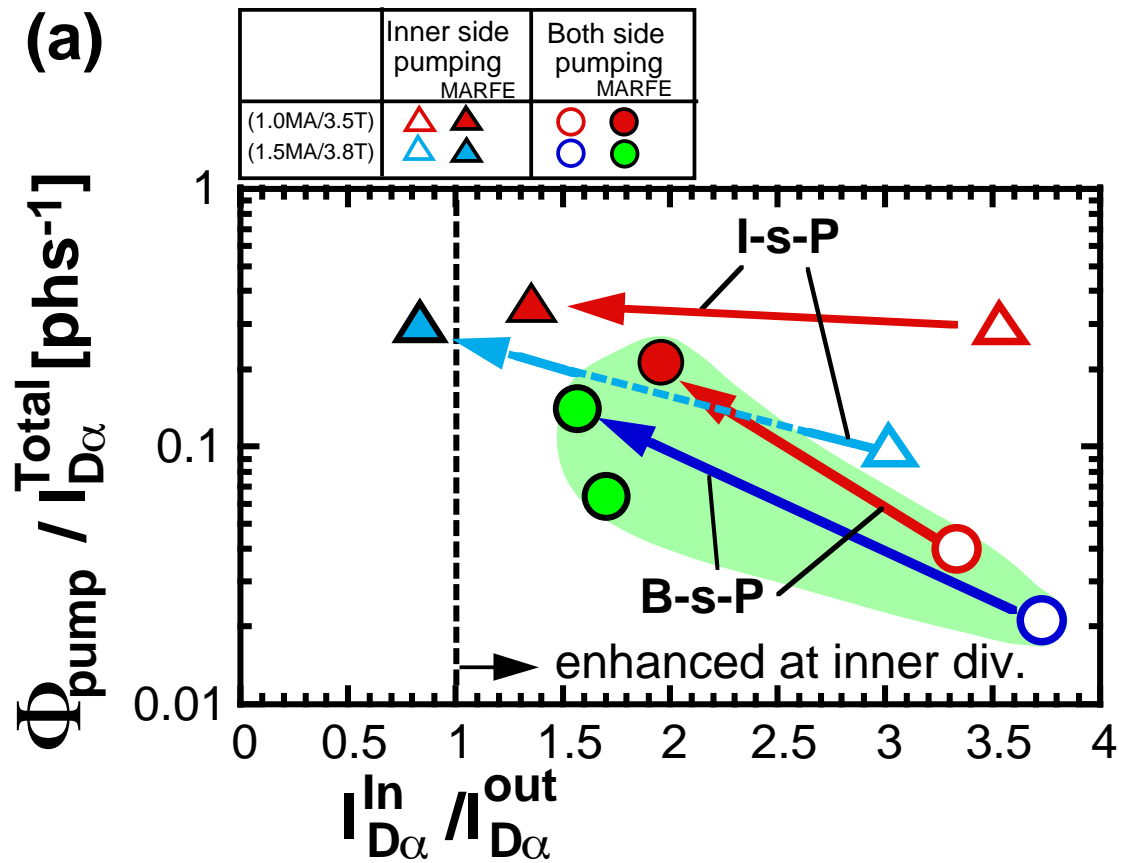


Fig. 2 asakura

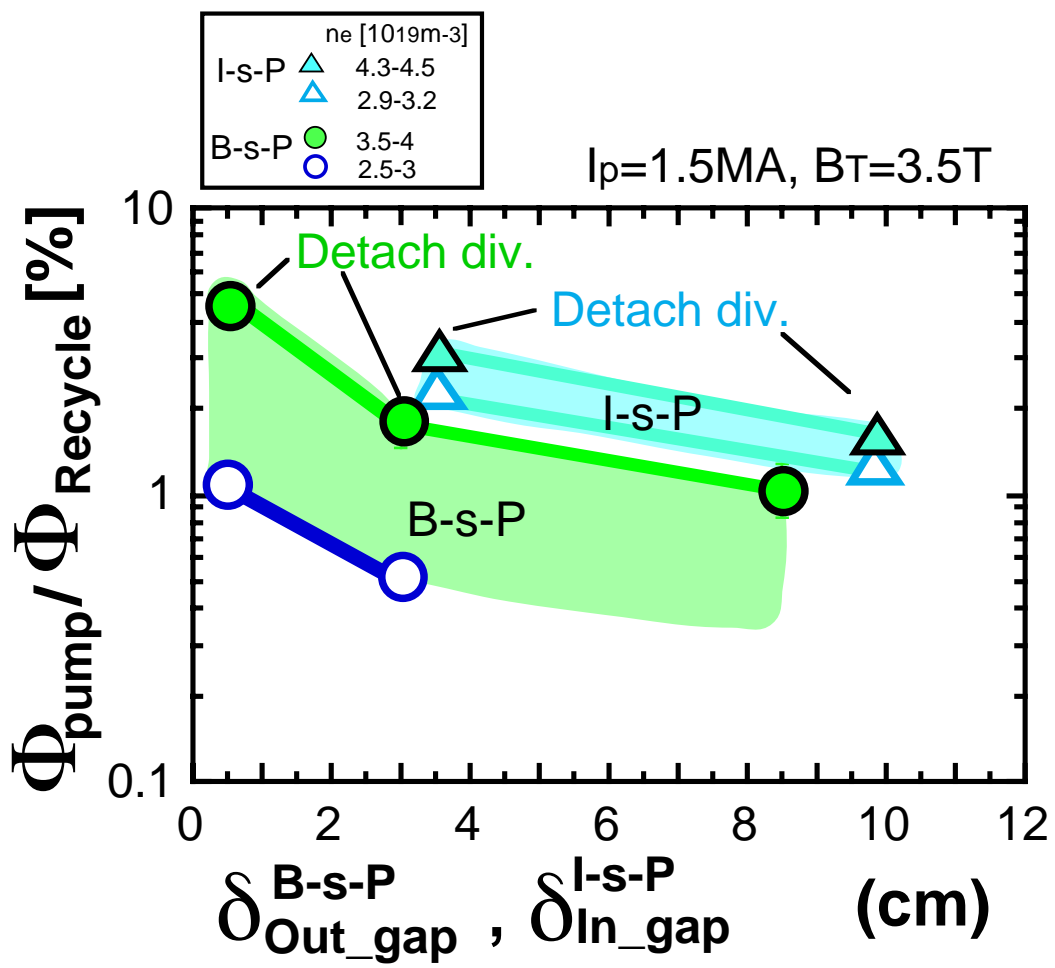
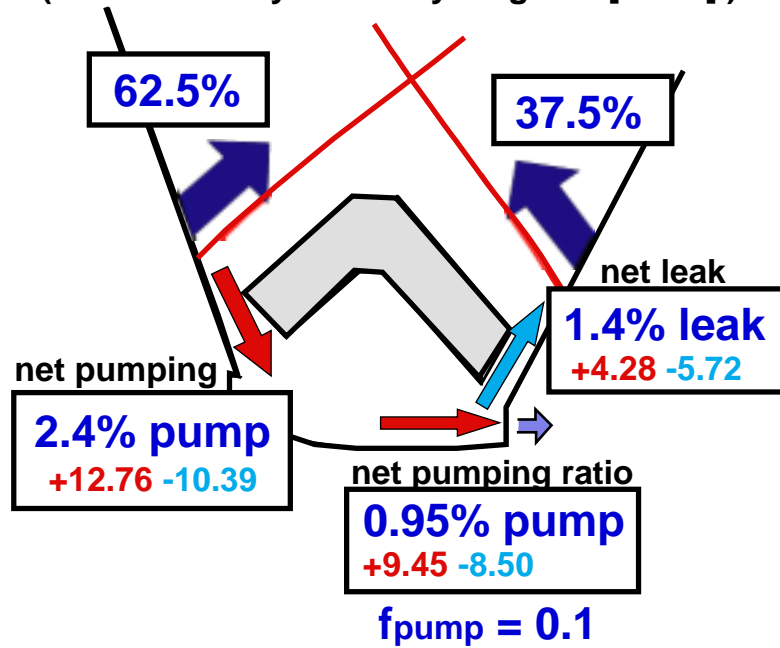


Fig.3 asakura

(a) Pumping ratio ($\delta_{g-In}, \delta_{g-Out} = 3\text{cm}$)
 (normalized by total recycling flux [100%])



(b) Pumping ratio ($\delta_{g-In} = 1, \delta_{g-Out} = 0.5\text{cm}$)

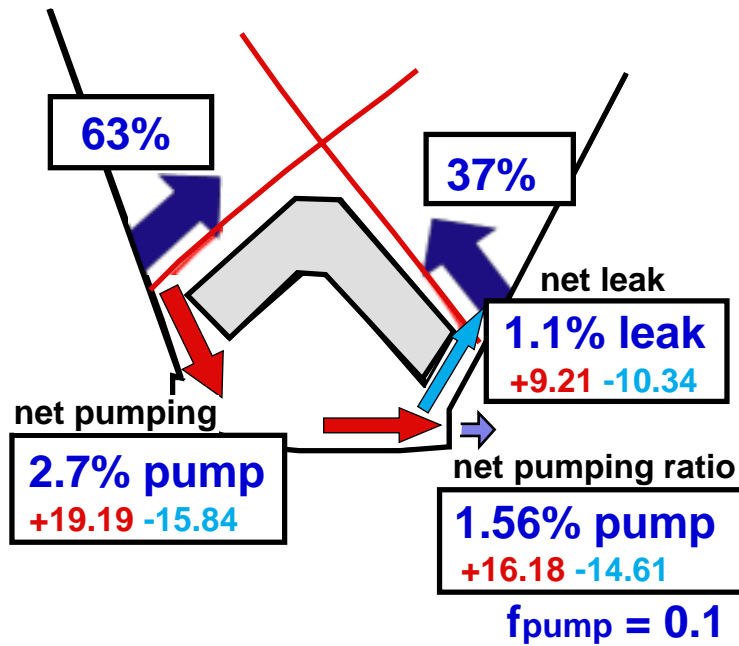


Fig.4 asakura

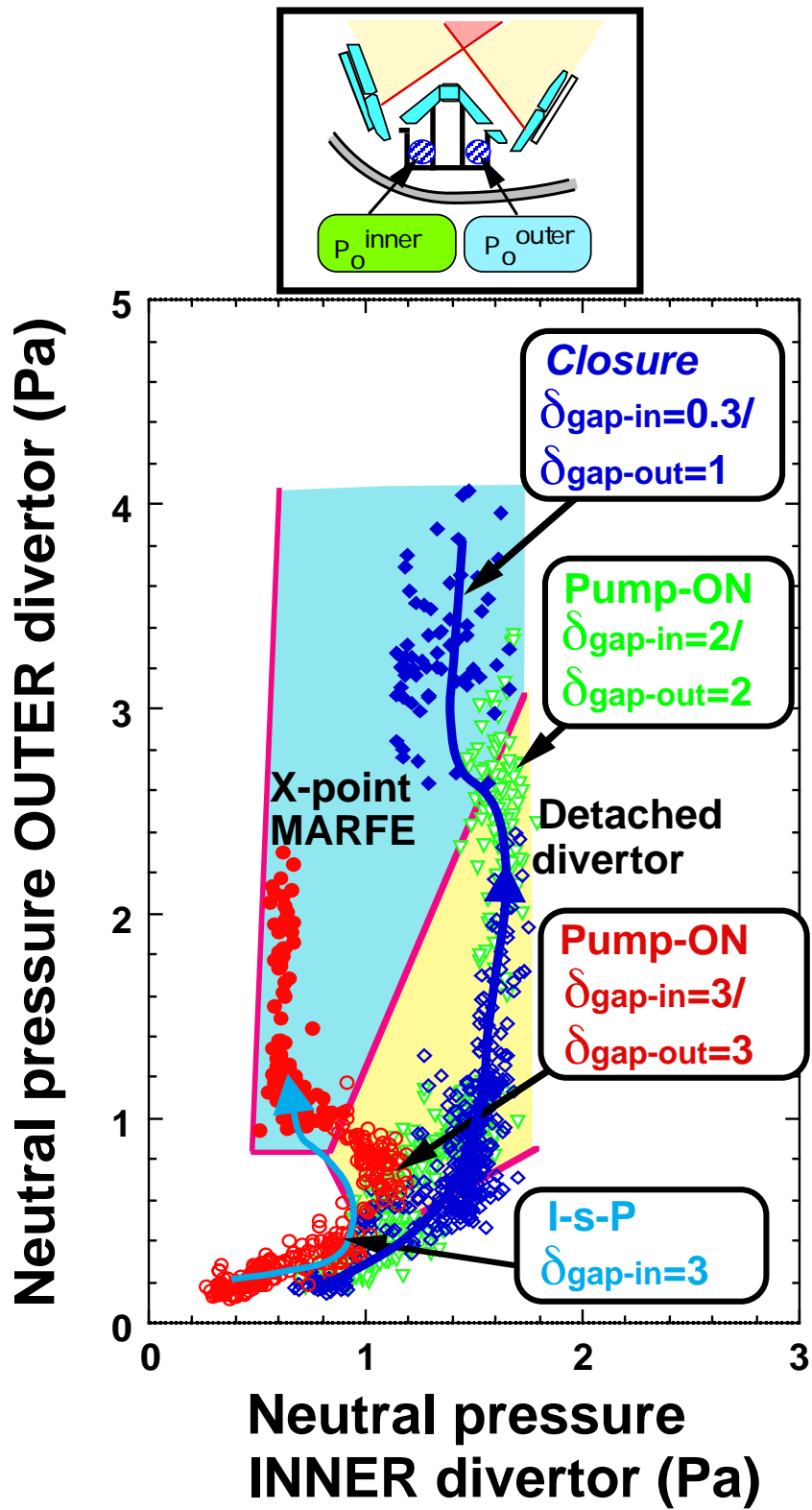


Fig.5 asakura

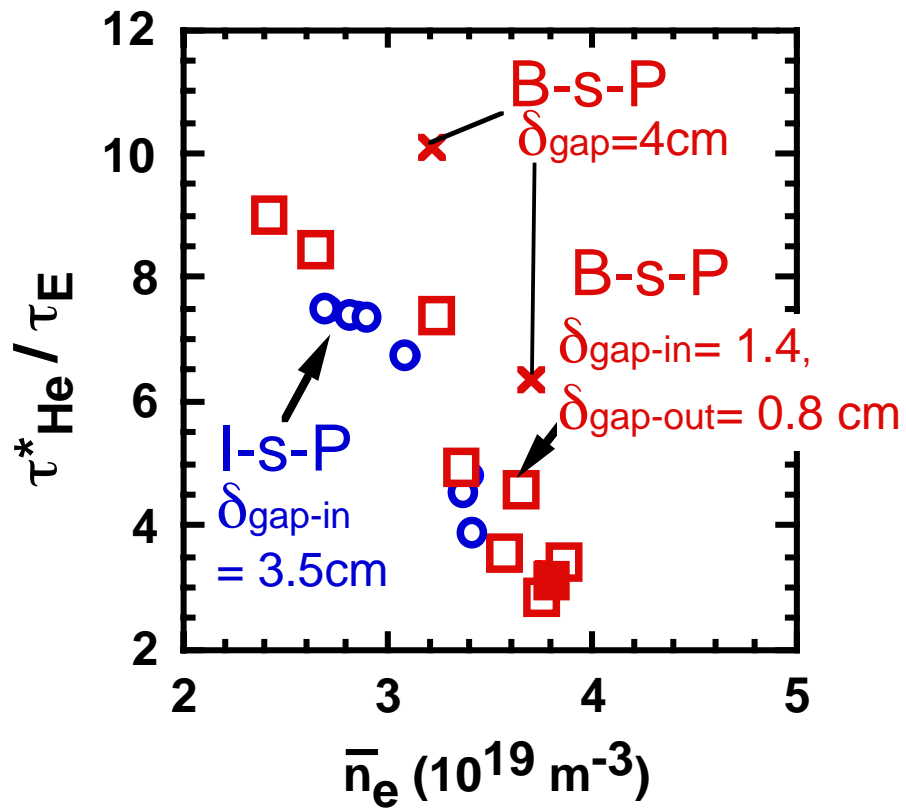


Fig.6 asakura

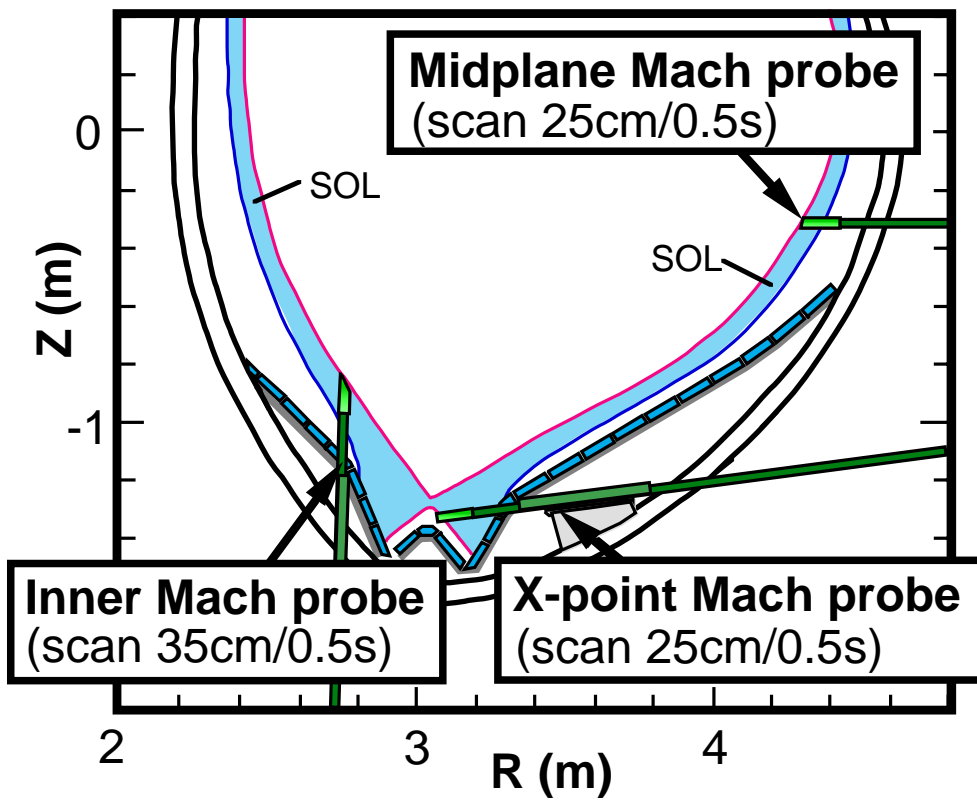


Fig.7 asakura

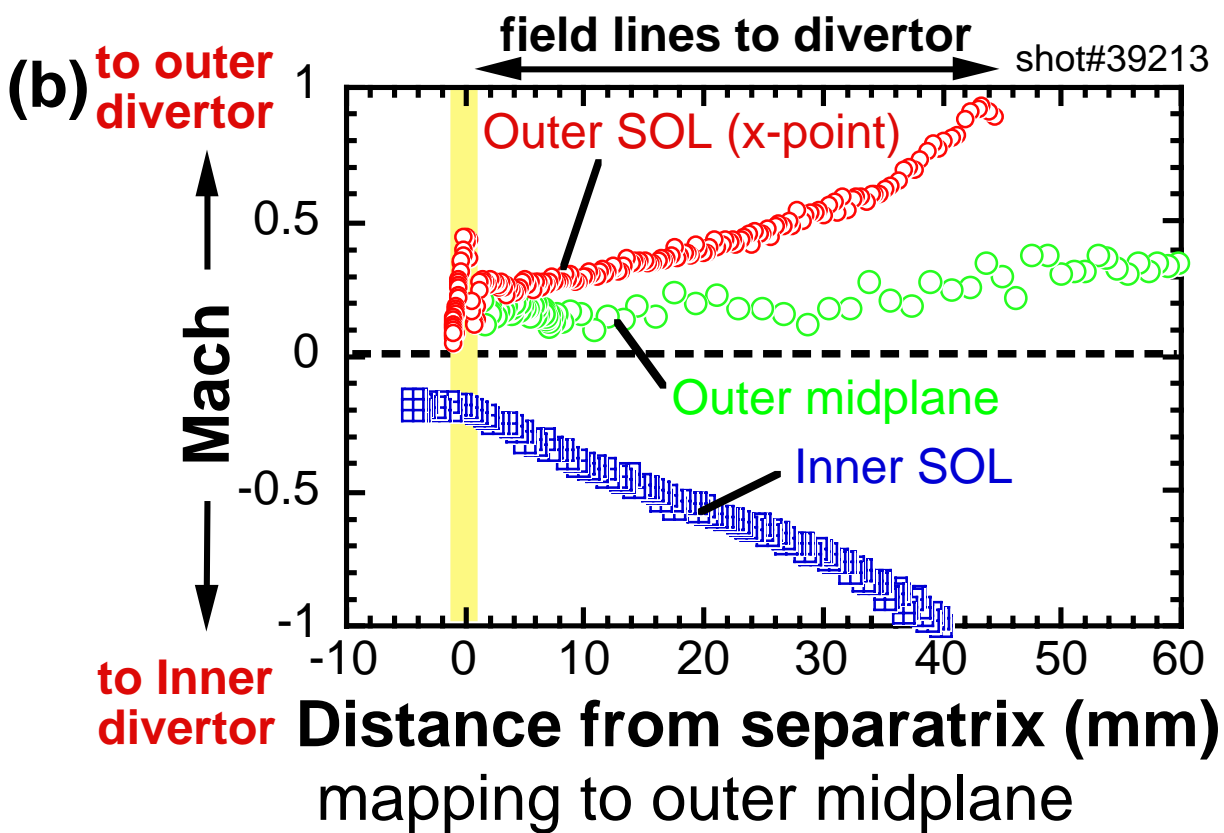
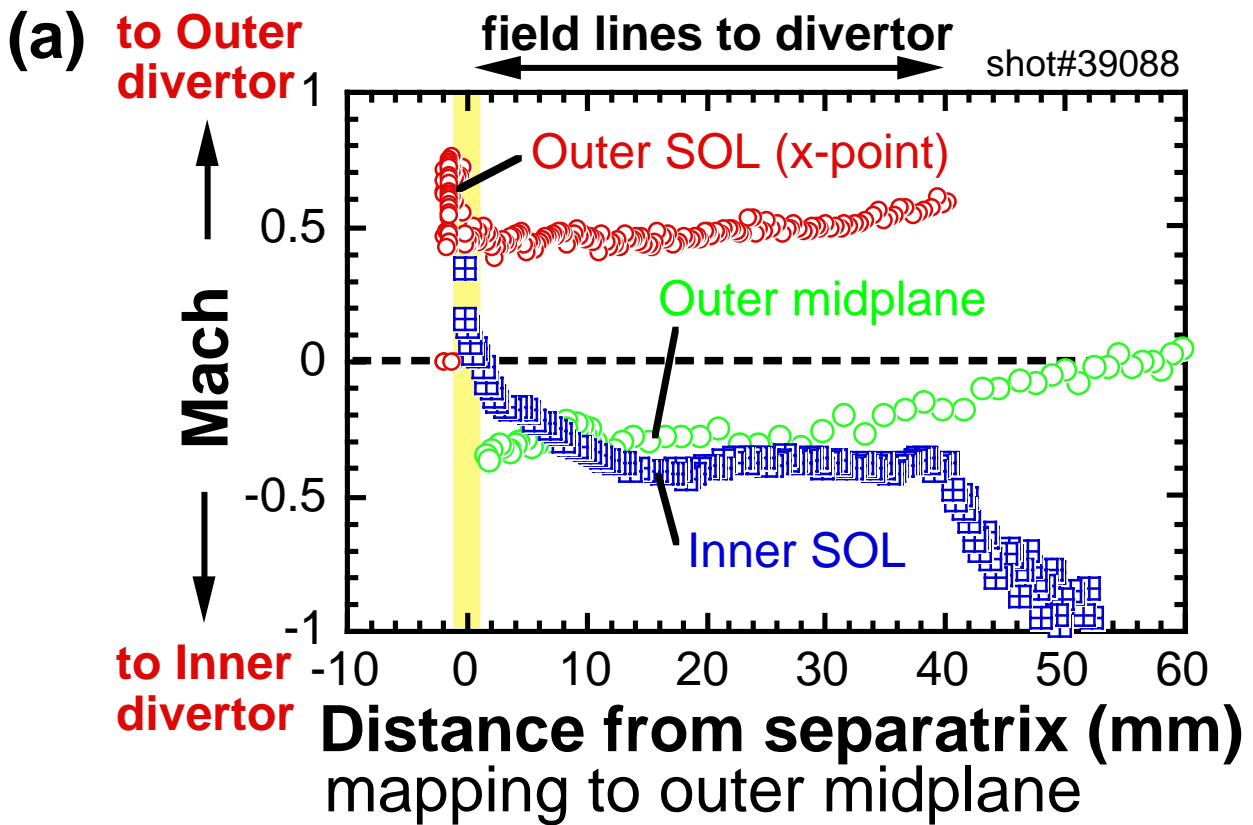


Fig.8 asakura

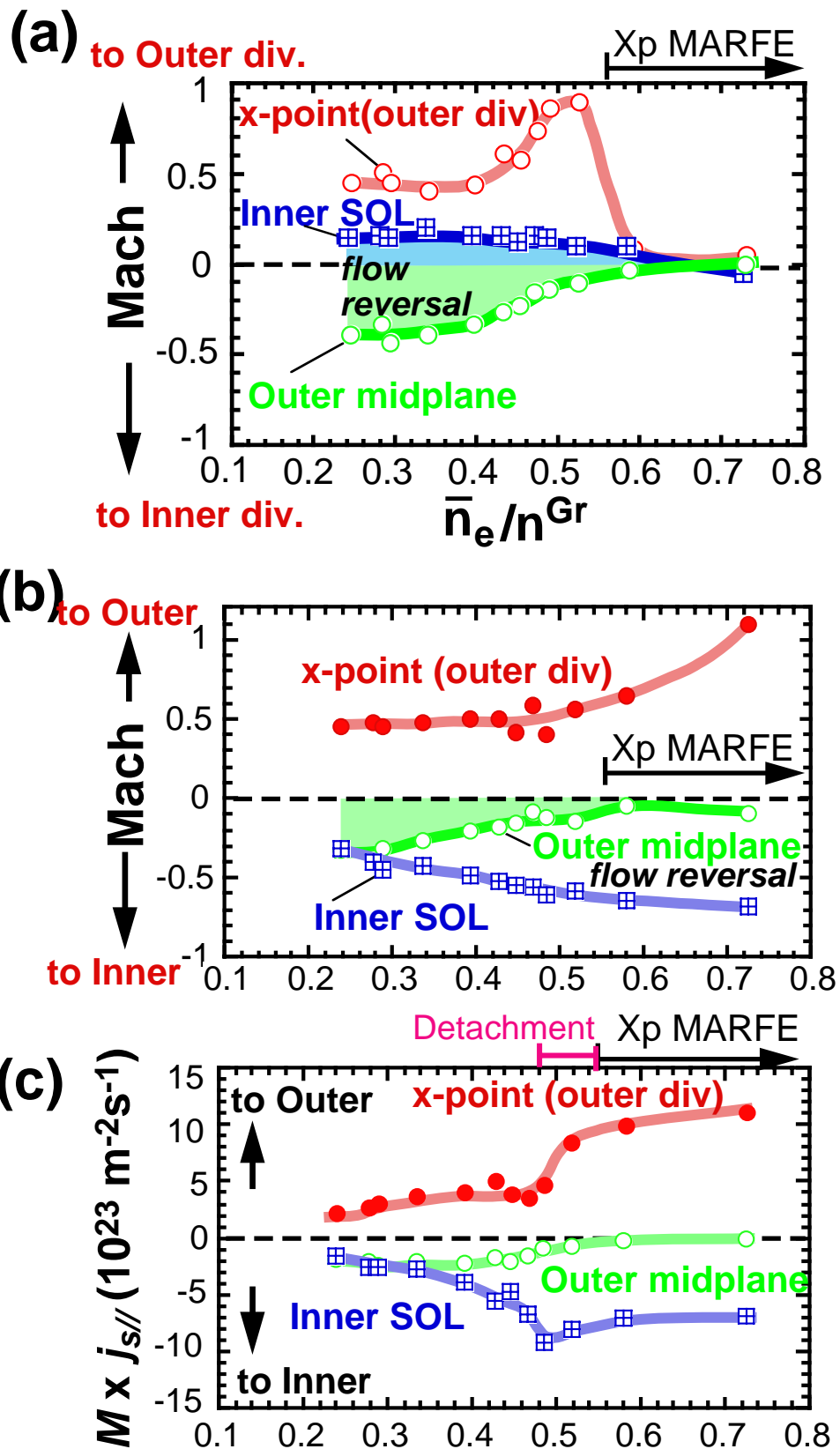


Fig.9 asakura

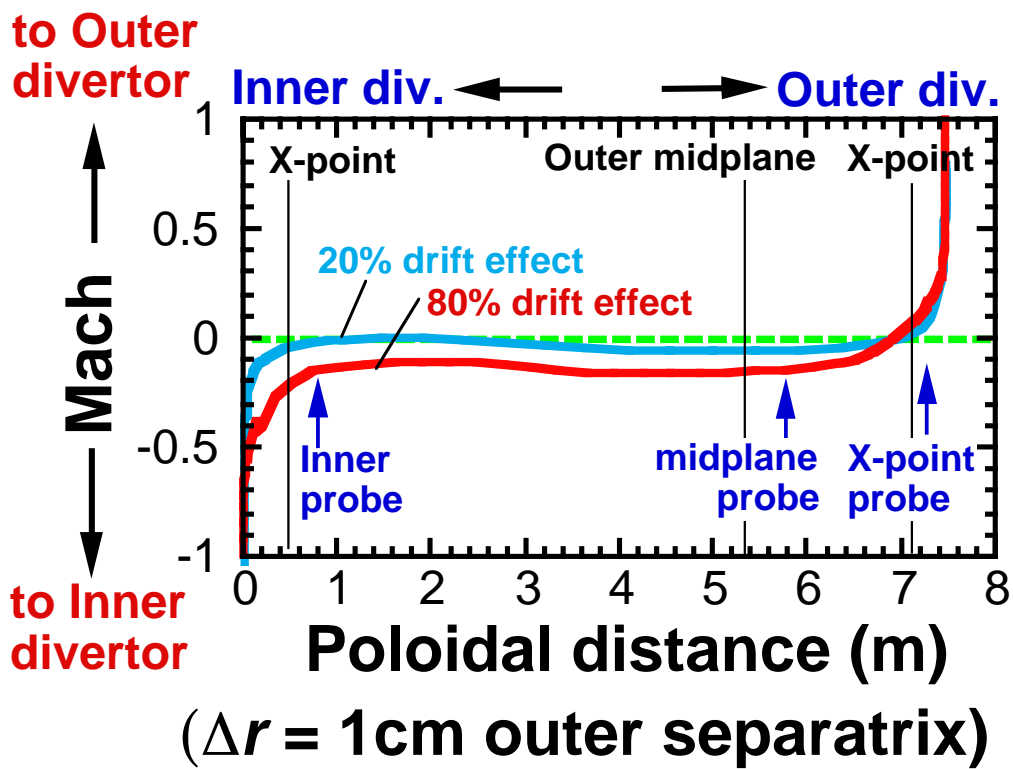


Fig.10 asakura

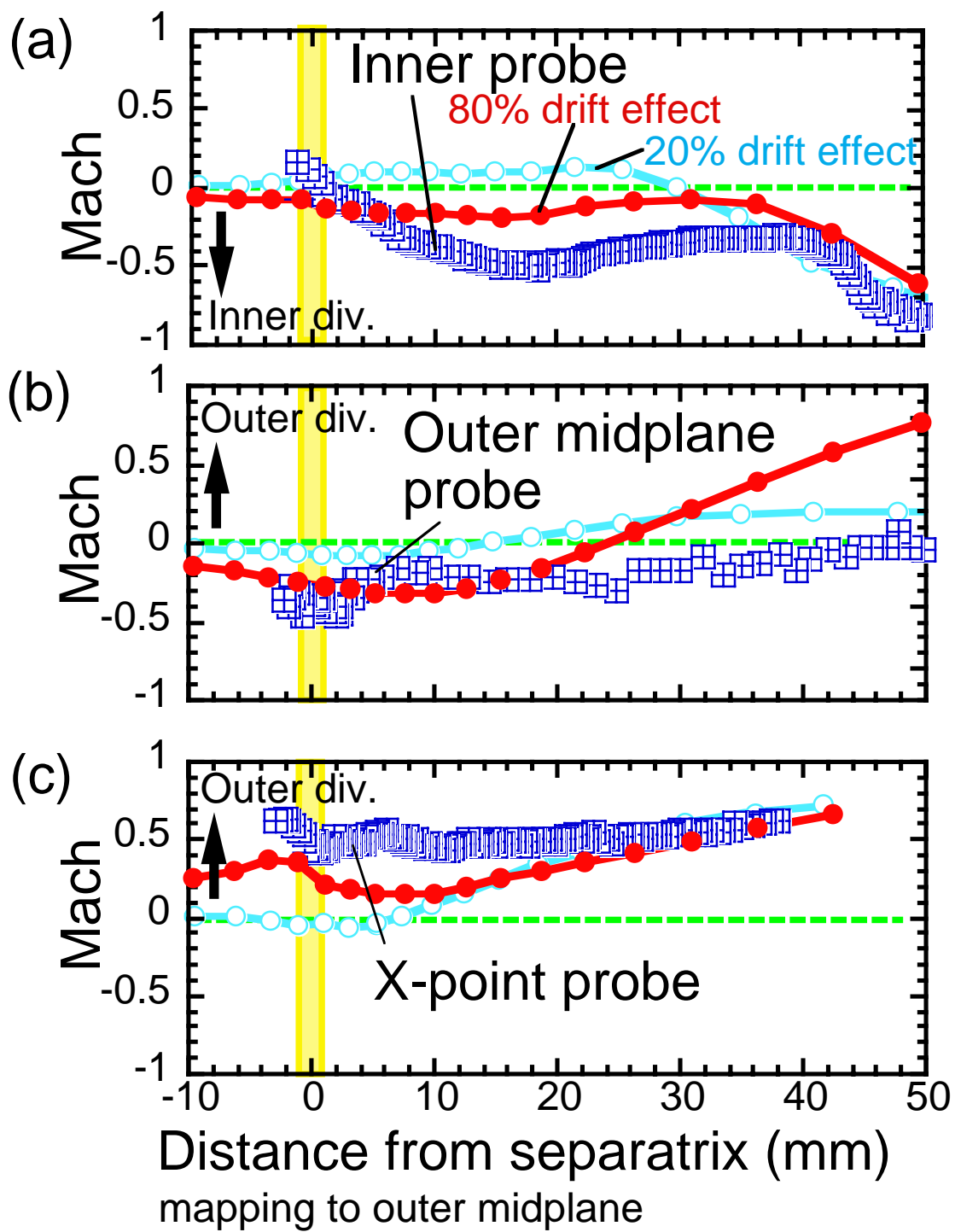


Fig.11 asakura